THE ASTROPHYSICAL JOURNAL, 812:139 (16pp), 2015 October 20 doi:10.1088/0004-637X/812/2/139

SIXTEEN YEARS OF *ULYSSES* INTERSTELLAR DUST MEASUREMENTS IN THE SOLAR SYSTEM. I. MASS DISTRIBUTION AND GAS-TO-DUST MASS RATIO

HARALD KRÜGER[1], PETER STRUB[1], EBERHARD GRÜN[2,3], AND VEERLE J. STERKEN[3,4]
[1] Max-Planck-Institut für Sonnensystemforschung, Justus-von-Liebig-Weg 3, D-37077 Göttingen, Germany; krueger@mps.mpg.de
[2] Laboratory for Atmospheric and Space Physics, University of Colorado, Boulder, CO, 80303-7814, USA
[3] Max-Planck-Institut für Kernphysik, Saupfercheckweg 1, D-69117 Heidelberg, Germany
[4] International Space Science Institute, Hallerstrasse 6, 3012 Bern, Switzerland
Received 2014 May 26; accepted 2015 September 6; published 2015 October 19

ABSTRACT

In the early 1990s, contemporary interstellar dust penetrating deep into the heliosphere was identified with the in situ dust detector on board the *Ulysses* spacecraft. Between 1992 and the end of 2007 *Ulysses* monitored the interstellar dust stream. The interstellar grains act as tracers of the physical conditions in the local interstellar medium (ISM) surrounding our solar system. Earlier analyses of the *Ulysses* interstellar dust data measured between 1992 and 1998 implied the existence of a population of "big" interstellar grains (up to 10^{-13} kg). The derived gas-to-dust-mass ratio was smaller than the one derived from astronomical observations, implying a concentration of interstellar dust in the very local ISM. In this paper we analyze the entire data set from 16 yr of *Ulysses* interstellar dust measurements in interplanetary space. This paper concentrates on the overall mass distribution of interstellar dust. An accompanying paper investigates time-variable phenomena in the *Ulysses* interstellar dust data, and in a third paper we present the results from dynamical modeling of the interstellar dust flow applied to *Ulysses*. We use the latest values for the interstellar hydrogen and helium densities, the interstellar helium flow speed *of* $v_{\mathrm{ISM}\infty} = 23.2\ \mathrm{km\ s^{-1}}$, and the ratio of radiation pressure to gravity, β, calculated for astronomical silicates. We find a gas-to-dust mass ratio in the local interstellar cloud of $R_{\mathrm{g/d}} = 193^{+85}_{-57}$, and a dust density of $(2.1 \pm 0.6) \times 10^{-24}\ \mathrm{kg\ m^{-3}}$. For a higher inflow speed of 26 km s^{-1}, the gas-to-dust mass ratio is 20% higher, and, accordingly, the dust density is lower by the same amount. The gas-to-dust mass ratio derived from our new analysis is compatible with the value most recently determined from astronomical observations. We confirm earlier results that the very local ISM contains "big" (i.e., $\approx 1\ \mu$m sized) interstellar grains. We find a dust density in the local ISM that is a factor of three lower than values implied by earlier analyses.

Key words: dust, extinction – interplanetary medium – ISM: abundances – ISM: general – meteorites, meteors, meteoroids – zodiacal dust

1. INTRODUCTION

The term "dust" is often considered as a synonym for dirt, which is annoying and difficult to quantify. Astronomers who observe distant objects in our Galaxy and beyond have to struggle with foreground obscuration due to the zodiacal light in our solar system, as well as with extinction by interstellar and even intergalactic dust. Therefore, dust is often considered a nuisance.

On the other hand, cosmic dust particles are involved in many astrophysical processes and play a crucial role in the cosmic life cycle of matter. They trace physical and chemical processes everywhere in the universe, ranging from the solar system at our doorstep to as far out as high-redshift galaxies. Cosmic dust provides the surface for complex chemical reactions and determines the thermal, ionization, and dynamical state of matter through its interaction with electromagnetic radiation, cosmic rays, and gas particles. Dust is not easily controlled; rather, it follows its own dynamics and disperses rapidly from its source. This aspect, however, has a positive side: like photons, dust particles carry information about remote processes through space and time, and the objects they originated from. This concept is called "Dust Astronomy," and modern dust observations are performed with a dust telescope on a dust observatory in space (Grün et al. 2004).

Interstellar dust became a topic of astrophysical research in the early 1930s when the existence of extinction, weakening, and scattering of starlight in the interstellar medium (ISM) was realized. At that time, astronomical observations provided the only information about the properties of dust in the ISM.

With the advent of dust detectors on board spacecraft, it became possible to investigate dust particles in situ. Around 40 yr ago, analysis of the data obtained with the dust instruments flown on a couple of spacecraft suggested that contemporary interstellar dust grains can cross the heliospheric boundary and penetrate deeply into the heliosphere (Bertaux & Blamont 1976; Wolf et al. 1976).

In the 1990s, this was undoubtedly demonstrated: the dust detector on board the *Ulysses* spacecraft, which measured mass, speed, and approach direction of the impacting grains, identified interstellar dust grains with radius above 0.1 μm that were flowing through the heliosphere (Grün et al. 1993, 1994, 1995b). These grains originated from the local interstellar cloud (LIC), which is the interstellar cloud surrounding our solar system. We follow the notation by Frisch et al. (1999). Details of the local interstellar setting of our solar system were also given by Redfield & Linsky (2008). The *Ulysses* measurements offered the opportunity to probe dust from the LIC.

The *Ulysses* interstellar dust measurements were later confirmed by the *Galileo* (Baguhl et al. 1996; Altobelli et al. 2005) and *Cassini* spacecraft (Altobelli et al. 2003, 2007, 2015), and interstellar impactors were also identified in the *Helios* dust data (Altobelli et al. 2006). In 2006, the *Stardust* mission successfully brought a sample of collected interstellar grains to Earth (Westphal et al. 2014). Finally, there are recent claims of detections of interstellar grains with radio and plasma wave instruments (Belheouane et al. 2012).

Measurements of interstellar dust inside the planetary system now provide a new window for the study of diffuse interstellar matter at our doorstep. However, the interstellar dust stream in the heliosphere is strongly modified from the undisturbed flow outside the heliosphere, in particular by solar radiation effects and the Lorentz force. These modifications have to be taken into account for a proper interpolation of the interstellar dust properties to the ISM outside the heliosphere where these grains originate from.

In addition to interstellar dust, various populations of dust originating from sources inside the solar system were investigated in interplanetary space with the *Ulysses* and *Galileo* dust experiments: the interplanetary dust complex, which is constantly replenished by dust from asteroids and comets (Grün et al. 1997), including β-meteoroids (i.e., dust particles that leave the solar system on unbound orbits owing to acceleration by radiation pressure; Hamilton et al. 1996; Wehry et al. 2004), and dust stream particles expelled from the Jovian system by electromagnetic forces (Grün et al. 1998), to name only the most significant dust types studied so far. For a summary of the *Ulysses* dust investigations in interplanetary space see Krüger et al. (2010, references therein). See also Krüger & Grün (2009), Mann (2010), Frisch et al. (2011), and Frisch & Slavin (2013) for recent reviews of measurements and modeling of interstellar dust in the heliosphere and beyond.

1.1. Interstellar Dust Entering the Heliosphere

The *Ulysses* in situ dust measurements obtained in the 1990s showed that the motion of interstellar grains through the solar system is—within the dust measurement accuracy—parallel to the flow of neutral interstellar hydrogen and helium gas. A speed of 26 $\mathrm{km\,s^{-1}}$ was adopted in these earlier analyses (Grün et al. 1994; Baguhl et al. 1995a; Witte et al. 1996; Witte 2004). The grains that originated from the very local interstellar environment of our solar system were identified by their impact direction and impact speed, the latter being compatible with particles moving on hyperbolic heliocentric trajectories (Grün et al. 1994). Their dynamics depend on the grain size and are strongly affected by the interaction with the interplanetary magnetic field (IMF) and by solar radiation pressure (Landgraf et al. 1999; Landgraf 2000; Mann & Kimura 2000; Czechowski & Mann 2003a, 2003b; Landgraf et al. 2003; Sterken et al. 2012, 2013a, 2015). Strong filtration of small grains due to electromagnetic forces also occurs at the heliospheric boundary (Linde & Gombosi 2000), leading to a strong modification of the size distribution and fluxes of grains measured inside the heliosphere. The interstellar dust flux modulation due to grain interaction with the IMF during solar minimum could be well explained by numerical simulations (Landgraf 1998, 2000; Landgraf et al. 2003).

The interstellar dust flow persists at high ecliptic latitudes above and below the ecliptic plane and even over the poles of the Sun, whereas interplanetary dust is strongly depleted at high latitudes (Grün et al. 1997). The interstellar dust flux measured at a distance of about 3 AU from the Sun is time dependent, and the mean mass of the grains is about 3×10^{-16} kg (Landgraf et al. 2000), corresponding to a grain radius of approximately 0.3 μm (assuming a grain density of 2.5 $\mathrm{kg\,m^{-3}}$). The earlier analyses of the *Ulysses* dust measurements yielded an upstream direction of the dust flow at 259° ecliptic longitude and 8° latitude (Landgraf 1998).

Spectroscopic observations of sightlines to stars enable information of intervening dust characteristics to be obtained. Studies of the dust impacts detected with both *Ulysses* and its twin dust detector on board *Galileo* indicated that the intrinsic size distribution of interstellar grains in the LIC extends to grain sizes larger than those detectable by such astronomical observations (Frisch et al. 1999; Grün & Landgraf 2000; Landgraf et al. 2000; Frisch & Slavin 2003). Observations of radar meteors entering the Earth's atmosphere at high speeds indicate the existence of even larger interstellar grains (Taylor et al. 1996; Baggaley & Neslušan 2002; Baggaley et al. 2007), although this conclusion remains under debate.

The *Ulysses* and *Galileo* interstellar dust measurements implied that the gas-to-dust mass ratio in the LIC is higher than the standard interstellar value derived from cosmic abundances (Landgraf 1998; Frisch et al. 1999; Kimura et al. 2003a). This implied the existence of inhomogeneities in the diffuse ISM on relatively small length scales ($\ll$1 kpc; Grün & Landgraf 2000).

Owing to its unique highly inclined heliocentric trajectory and very long mission duration, *Ulysses* was able to monitor the interstellar dust flow through the solar sytem over 16 yr. This time period covers more than two and a half revolutions of the spacecraft about the Sun through more than 2/3 of a complete 22 yr (magnetic) solar cycle (Figure 1). Thus, *Ulysses* measured interstellar dust during solar minimum and solar maximum conditions of the IMF.

Earlier comprehensive investigations of the interstellar impactors were mostly performed in the late 1990s and relied on the significantly smaller data set available at the time. Until the end of the *Ulysses* mission, the interstellar dust data set has grown by more than a factor of two, so that a complete reanalysis is worthwhile and can give new insights into, e.g., the grain dynamics inside the heliosphere and into the conditions in the local interstellar environment where these grains originate.

Recent measurements with the *Interstellar Boundary Explorer* (*IBEX*) spacecraft led to a revision of the interstellar gas flow vector (speed and direction) derived earlier from *Ulysses* measurements (Witte 2004, inflow speed $v_{\mathrm{ISM}\infty} = 26\ \mathrm{km\,s^{-1}}$). The *IBEX* measurements of the interstellar flow are also more consistent with newer and independent astronomical measurements (Redfield & Linsky 2008). *IBEX* showed that the Sun is still located within the LIC. The inflow speed of the ISM as derived by *IBEX* is $v_{\mathrm{ISM}\infty} = 23.2\ \mathrm{km\,s^{-1}}$, and the downstream flow direction is $l_{\mathrm{ISM}\infty} = 79°$ ecliptic longitude and $b_{\mathrm{ISM}\infty} = -5°$ ecliptic latitude (McComas et al. 2012). Given that the impact speed of the dust grains affects the mass calibration of our interstellar dust measurements, we analyze the *Ulysses* data in view of this reduced inflow speed. However, this speed *was*, like the direction, under debate (Lallement & Bertaux 2014; McComas et al. 2015; Wood et al. 2015). The higher inflow speed of $v_{\mathrm{ISM}\infty} = 26\ \mathrm{km\,s^{-1}}$ increases our derived gas-to-dust mass ratio by about 20% (see Section 5).

This is the first in a series of three papers dedicated to the analysis of the full *Ulysses* data set of 16 yr of interstellar dust measurements in the heliosphere. In this paper we review the mass distribution of interstellar grains detected in the heliosphere. Temporal variations in dust flux, impact direction, and grain size during this time period are investigated by Strub

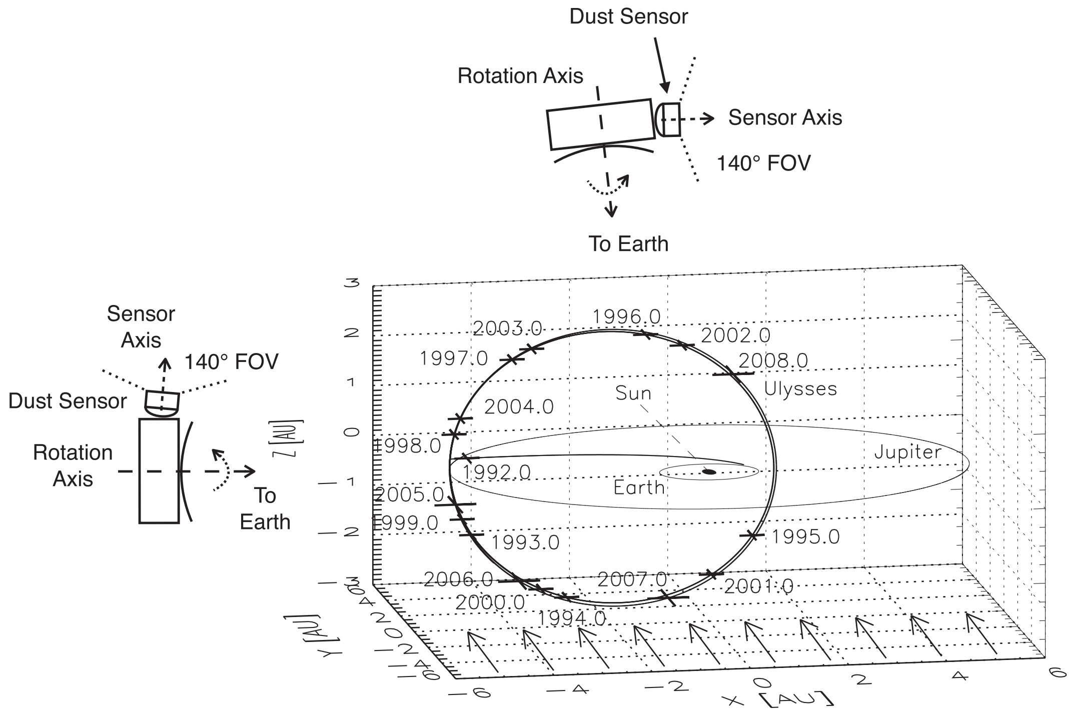

Figure 1. Trajectory of *Ulysses* in ecliptic coordinates with the Sun at the center. The orbits of Earth and Jupiter indicate the ecliptic plane, and the initial trajectory of *Ulysses* was in this plane. After Jupiter flyby in early 1992, the orbit was almost perpendicular to the ecliptic plane (79° inclination). Crosses mark the spacecraft position at the beginning of each year. Vernal equinox is to the right (positive x-axis). Arrows indicate the undisturbed interstellar dust flow direction, which is within the measurement accuracy co-aligned with the direction of the interstellar helium gas flow. It is almost perpendicular to the orbital plane of *Ulysses*. The *Ulysses* spacecraft and the scan orientation of the dust detector are sketched for two positions along the orbit: at aphelion and at the spacecraft's highest ecliptic latitude.

et al. (2011, 2015), and results from modeling of grain dynamics in the context of the observations are presented by Sterken et al. (2015). In Section 2 we briefly describe the *Ulysses* mission, the *Ulysses* dust detector, and its operation. In Section 3 we derive the *Ulysses* interstellar dust data set, and in Section 4 we obtain the mass distribution of interstellar grains and the gas-to-dust mass ratio in the LIC. Section 5 provides a discussion, and in Section 6 we summarize our conclusions.

2. THE *ULYSSES* DUST INSTRUMENT

The *Ulysses* dust instrument detects individual dust particles impacting onto the sensor target, measures their mass and impact speed, and determines the impact direction (Grün et al. 1992b). Up to now *Ulysses* was the only space probe that left the ecliptic plane and passed over the poles of the Sun. *Ulysses* was launched in 1990 October. After a swing-by maneuver at Jupiter in 1992 February, the spacecraft's orbital plane was almost perpendicular to the ecliptic plane (79° inclination), with an aphelion at Jupiter and a 6 yr period (Figure 1). Subsequent aphelion passages occurred in 1998 April and in 2004 June. This special orbit orientation allowed the dust detector on board *Ulysses* to unambiguously detect interstellar dust grains entering the heliosphere because the spacecraft's orbital plane was almost perpendicular to the flow direction of the interstellar dust (Figure 1). *Ulysses* was operated until 2009.

A practically identical twin instrument was operated on board the *Galileo* spacecraft, which was launched in 1989, and between 1995 and 2003 it was the first Jupiter-orbiting spacecraft (Grün et al. 1992a). A third identical instrument (GORID), an engineering model of the *Ulysses* sensor, was operational in geostationary orbit on the *Express* telecommunication satellite between 1997 and 2002 (Drolshagen et al. 1999). Finally, the *Cassini* spacecraft, launched in 1997, carries the Cosmic Dust Analyzer (CDA), which is an upgrade of the *Ulysses* instrument that is equipped with a time-of-flight mass spectrometer (Srama et al. 2004). *Cassini* has been successfully measuring dust in the Saturnian system since 2004. Altogether, these four instruments very successfully collected cosmic dust measurements during more than 50 yr in space.

2.1. *Impact Ionization*

The physical mechanism most generally utilized in modern spaceborne in situ detectors of cosmic dust is based on the measurement of the electric charge generated upon impact of a fast projectile onto a solid target (impact ionization; Raizer 1960; Friichtenicht & Slattery 1963). It yields the highest sensitivity for the detection of dust particles in space (see Auer 2001, for a review). The electrical charge generated upon particle impact can be quantitatively calibrated to provide impact speed and mass of the grains. The impacts can be detected by several independent measurements on different instrument channels (multi-coincidence detection), which allows for a reliable dust impact detection and identification of noise events. In combination with a time-of-flight mass spectrometer, an impact ionization detector can measure the chemical composition of the impacting grains.

When a dust particle strikes a solid target with high speed ($\gg 1\ \mathrm{km\ s^{-1}}$), it produces a crater in the target and ejecta composed of both particle and target material. The ejecta consist of positive and negative ions, electrons, and neutral atoms and molecules originating from both projectile and target. Because of its high internal pressure (up to 5 TPa), the

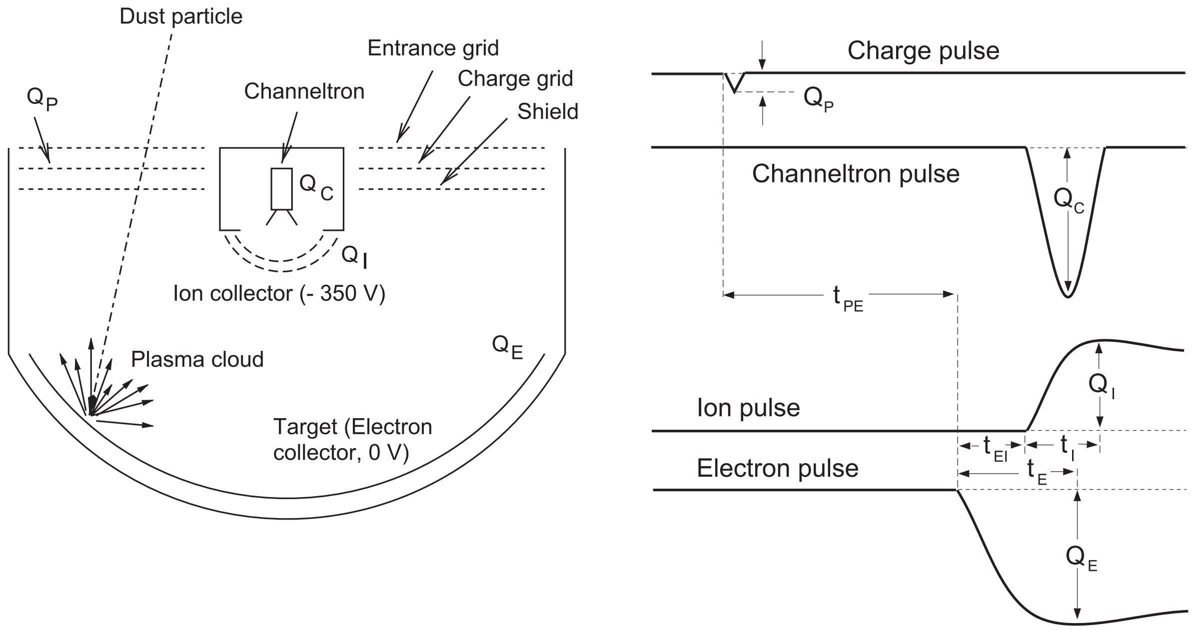

Figure 2. Schematic sensor configuration of the *Ulysses* dust detector (left) and charge signals measured upon impact of a negatively charged dust particle (right). From Grün et al. (1992a).

ejecta cloud expands rapidly into the surrounding vacuum. As the ejecta strike sensor side walls and other surfaces, they produce secondary ions, electrons, and debris, which, in turn, can strike more surfaces and produce additional ejecta.

The experimental arrangement typically consists of a metal target plate and a collector (e.g., a metal grid) for either the ions or electrons of the impact plasma. The target is preferentially made of a material with a high electron yield like molybdenum, tantalum, tungsten, or gold. Different electric potentials applied to the target plate and the collector generate an electric field, separating the positively and negatively charged particles of the plasma. Charge-sensitive amplifiers coupled to both the target plate and the collector register independently, but simultaneously, an impacting dust particle. The total amount of charge, Q, collected on each channel is a function of mass m and impact speed v of the particle, as well as the particle's composition. Q can be described by the empirical law

$$Q \propto m^{\alpha}\, v^{\gamma}, \tag{1}$$

with $\alpha \simeq 1$ and $1.5 \lesssim \gamma \lesssim 5.5$ in the speed range $2\,\mathrm{km\,s^{-1}} \lesssim v \lesssim 70\,\mathrm{km\,s^{-1}}$ (Auer 2001). In particular, for constant impact speed, the charge generated upon impact is proportional to the particle mass (Göller & Grün 1985).

The rather wide range in γ is due to different impact speeds, target and projectile materials, and collector geometries used for the measurements. In particular, the physical processes involved are speed dependent, and the impact ionization process is often divided into three speed regimes, characterized by different values of γ (Stübig 2002). At speeds below about $6\,\mathrm{km\,s^{-1}}$ surface ionization dominates ($3.5 \lesssim \gamma \lesssim 4.5$): the surfaces of the solid bodies involved in the impact process are heated by the impact shock, leading to thermal ionization of the surfaces. In addition, ionization of alkali contaminants on the target, having low ionization potentials, takes place. In the high impact speed regime, above $18\,\mathrm{km\,s^{-1}}$, target and projectile ionization (volume ionization) dominates ($3.0 \lesssim \gamma \lesssim 5.5$). For intermediate speeds the charge yield is reduced owing to energy consumption by melting and vaporization processes ($1.5 \lesssim \gamma \lesssim 2.5$).

A similar behavior was also reported by Göller & Grün (1989). Owing to the large uncertainties in the exponent and material dependencies, these authors used a value of $\gamma = 3.5$ throughout the entire speed range to calibrate the *Ulysses* dust instrument. Here we use the empirical calibration curve of Grün et al. (1995b, their Table 4(c)), which was derived from impact experiments at a dust accelerator with iron, zinc-coated silica, and carbon particles.

The second important variable for the determination of the impact parameters is the rise time of the charge signal. It depends only on the impact speed of the particles (Dietzel et al. 1973). The rise time can be used to determine the impact speed when it is in the range of $1\,\mathrm{km\,s^{-1}} \lesssim v \lesssim 20\,\mathrm{km\,s^{-1}}$.

In addition to mass and speed, the composition of the ions in the plasma cloud can be determined with a time-of-flight mass spectrometer separating the ions according to their mass. The *Ulysses* dust instrument does not have a time-of-flight mass spectrometer, contrary to the dust instrument on board *Cassini* (Srama et al. 2004), which is an upgrade of the *Ulysses* instrument.

2.2. Instrument Description

The dust instrument on board *Ulysses* consists of a cylindrical sensor (with diameter 442 mm and length 301 mm) with channeltron and pre-amplifiers, signal conditioning, and spacecraft interface electronics. The sensor and the charge signals measured upon impact of a dust particle are schematically shown in Figure 2.

The sensor consists of a grid system for the measurement of the particle charge, an electrically grounded hemispherical gold-coated metal target, and a negatively biased ion collector grid. A charged dust particle entering the sensor induces a charge in the charge grid, which is measured by a charge-

Table 1
Parameters Measured by the Dust Instrument upon Impact of a Dust Particle onto the Sensor and Related Parameters

Parameter/ Digital Value	Measured Quantity	Range	Accuracy (Logarithmic Steps)	Related Particle Parameters
Q_E/EA	Negative charge (electrons)	10^{-14}–10^{-8} C	48	Mass, speed
Q_I/IA	Positive charge (ions)	10^{-14}–10^{-8} C	48	Mass, speed
Q_C/CA	Positive charge (partially)	10^{-13}–10^{-9} C (channeltron output)	32	Impact identification
Q_P/PA	Induced charge			Electric charge
	positive	10^{-14}–10^{-12} C	16	
	negative	10^{-14}–10^{-10} C	32	
t_E/ET	Rise time of negative charge	10–100 μs	16	Speed
t_I/IT	Rise time of positive charge	10–100 μs	16	Speed
t_{EI}/EIT	Time difference negative & positive charge signals	−5–44 μs	16	Impact identification
t_{PE}/PET	Time difference induced & negative charge signals	1–400 μs	32	Speed

Note. From Grün et al. (1995b).

sensitive amplifier. Once the particle hits the target, it generates electrons and ions that are separated by the electric field of −350 V between the hemisphere and the ion collector. The negative charges (electrons and negative ions, Q_E) are collected at the hemisphere and measured by a charge-sensitive amplifier. Positive ions (Q_I) are collected and measured at the negatively biased ion collector with a charge-sensitive amplifier. The ion collector has a transparency of about 40% so that some of the ions can penetrate the ion collector, are further accelerated, and are detected by an electron multiplier (channeltron). Secondary electrons are produced in the channeltron, amplified, and measured by a charge-sensitive amplifier (Q_C). Other parameters measured upon impact are the rise times t_I and t_E of both the positive and the negative charge pulses Q_I and Q_E. The measured time delay t_{EI} between the electron and ion pulses is used to distinguish true dust impacts from noise events (Baguhl et al. 1993). Dust impacts have time delays of 2–44 μs, while mechanical noise has a time delay of milliseconds. The thresholds and dynamic ranges of the various signals measured upon impact are given in Table 1.

A measurement cycle of the instrument can be initiated if one or more of the signals Q_E, Q_I, or Q_C exceeds an adjustable threshold. During normal operation, an event is initiated by the signals Q_I or Q_C. Because of high noise rates encountered for the electron channel, Q_E, this channel was not selected to initiate a measurement cycle.

The parameters of a single recorded event listed in Table 1 are digitized and stored in an Experiment Data Frame. Coincidences between various event signals, event time, and sensor pointing direction during the event, as well as status information (housekeeping data), are also recorded for each event. These data are transmitted to Earth and, in an initial step, used to determine whether the event was a true dust impact or a noise event. If the measured signals were due to a dust impact, the particle mass m and impact speed v are derived from the instrument calibration. No instrinsic dust charges were derived from the measured Q_P signals (Section 2.3). More detailed descriptions of the dust instrument, the reduction of the *Ulysses* dust data, and the identification of noise events are given by Grün et al. (1992a, 1992b, 1995b) and Baguhl et al. (1993).

2.3. Instrument Calibration

Before an instrument is carried into space, it must be tested on the ground to verify and calibrate its response. The most striking characteristic of dust particles detected in space is their high speed, which is typically in the range of 1–100 km s^{-1}. Their sizes are in the range 0.01–10 μm. Thus, in order to calibrate a dust instrument to be flown on a space mission, one has to accelerate particles in this size range to comparable speeds.

The only technique with which this speed and mass range is accessible is electrostatic acceleration (Fechtig et al. 1978; Auer 2001). This technique is based on the acquisition of kinetic energy by a particle of mass m and positive charge q falling through a potential difference U: $\frac{1}{2}mv^2 = qU$, where v is the terminal speed of the particle. Since the acceleration voltage can easily be measured, and v and q can be measured with pickup electrodes, the mass can be calculated for each accelerated particle.

In an electrostatic accelerator only conducting particles can be accelerated. Either the particle material must be a conductor, or the particle must be coated with a conducting material. Materials used for the calibration of the *Ulysses* detector were iron, carbon, and zinc-coated silica (Göller & Grün 1989). Calibration experiments for the *Cassini* dust instrument were also performed with coated latex particles (Stübig et al. 2001; Stübig 2002). Recently, metal- and polymer-coated particles could also be used for calibration experiments (Hillier et al. 2009, 2014), and first shots with porous particle analogs have been and are currently being attempted (Sterken et al. 2013b, 2015).

The calibration experiments of the *Ulysses* dust detector were performed at the Heidelberg dust accelerator facility (Göller & Grün 1985; Göller & Grün 1989), which is an electrostatic accelerator with a 2 MV van de Graaf high-voltage generator. The particles were in the speed range $1\ \mathrm{km\,s^{-1}} \leqslant v \leqslant 70\ \mathrm{km\,s^{-1}}$ and in the mass range $10^{-18}\ \mathrm{kg} \leqslant m \leqslant 10^{-13}\ \mathrm{kg}$. In addition to three different particle materials, tests with varying impact angles were also performed.

2.3.1. Speed and Mass

The particle speed can be determined from the rise times t_I and t_E of the charge signals measured on the ion collector and on the target. Grün et al. (1995b) measured the rise times of the impact signals as a function of impact speed for three different materials. The signal strength depends moderately on the particle material and also on the impact angle. Neither the particle material nor the impact angle is known for an impinging micrometeoroid. Therefore, averaged calibration curves are used to obtain impact speeds, assuming that the materials used for calibration represent cosmic dust particles of either iron, rock, carbonaceous, or CHON composition. Since the two rise times are measured independently, one obtains two (often different) speed values, v_{t_I} and v_{t_E}. The impact speed is taken as the geometric mean of both values: $v = \sqrt{v_{t_I} \cdot v_{t_E}}$. The typical accuracy of the derived speed v is a factor of 2.

Once the particle speed has been determined, its charge-to-mass ratio can be derived from the calibration curves obtained by laboratory impact experiments (Grün et al. 1995b). From these values and the corresponding impact charges Q_E and Q_I, two independent estimates of the mass m_{Q_E} and m_{Q_I} are derived. The particle mass is usually taken as the geometric mean $m = \sqrt{m_{Q_E} \cdot m_{Q_I}}$. If the speed is well determined, the mass can also be derived with a higher accuracy. The typical uncertainty in the mass m is a factor of 10. In this paper we derive the grain mass only from the charge Q_I measured on the ion collector.

The speed-dependent measurable mass range of the instrument is shown in Figure 3. During the close Jupiter flyby in 1992, the electronic detection threshold was set to a higher value because an increased noise level was expected (Grün et al. 1995a). In this case the sensitivity was reduced.

Since the charge-sensitive amplifiers covered six orders of magnitude in impact charge (and so did the mass range), the upper limit of the calibrated range is also indicated in Figure 3. For larger particles the instrument operated as a threshold detector (saturation range). The calibration covered a speed interval $2\ \mathrm{km\,s^{-1}} \lesssim v \lesssim 70\ \mathrm{km\,s^{-1}}$. Owing to the speed-dependent mass threshold, the mass range accessible by the instrument was $10^{-19}\ \mathrm{kg} \lesssim m \lesssim 10^{-9}\ \mathrm{kg}$.

The instrument calibration obtained in the laboratory was confirmed by measurements in the close vicinity of Jupiter's Galilean moons (Krüger et al. 1999b). The moons are surrounded by clouds of ejecta dust grains kicked up from their surfaces. The average impact speeds of these, most likely icy, grains were 6–8 $\mathrm{km\,s^{-1}}$ and were very close to the expected speeds. Particle sizes were 0.5–1.0 μm (Krüger et al. 2000, 2003), which is within the well-calibrated range of the instrument. On the other hand, the Jovian dust streams first detected in interplanetary space and later extensively studied in the Jovian magnetosphere consist of much smaller and faster particles, far beyond the calibrated range of the instrument (Zook et al. 1996): grain radii were actually about 10 nm, and their speeds exceeded 200 km $\mathrm{s^{-1}}$. These particles strongly interact with the interplanetary and the Jovian magnetic fields (Grün et al. 1998; Flandes et al. 2011), and they originate from Jupiter's moon Io (Graps et al. 2000). They are not the subject of this paper.

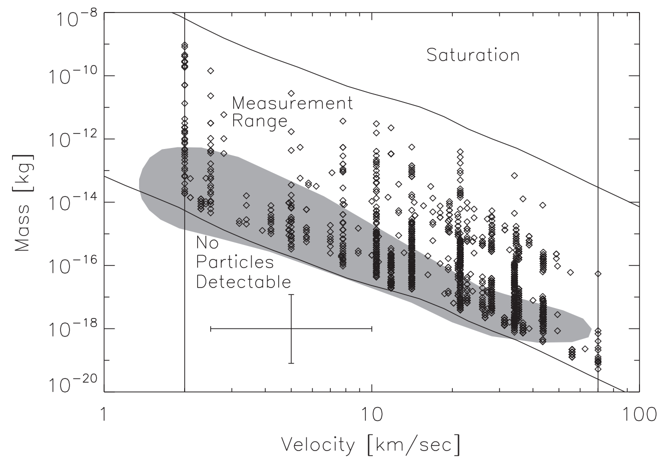

Figure 3. Calibrated mass and speed range of the *Ulysses* dust detector. In the region marked "Saturation" the instrument operates as a threshold detector. The shaded area shows the range where the instrument was calibrated in the laboratory. Below 2 km $\mathrm{s^{-1}}$ and above 70 km $\mathrm{s^{-1}}$ speeds and masses cannot be determined. The bottom cross represents typical accuracies of speed and mass values. Plus signs show the calibrated masses and speeds of 2113 particles measured with *Ulysses*. Jupiter stream particles are not shown as they are actually smaller and faster than the calibrated range of the instrument. Adapted from Grün et al. (1992a).

2.3.2. Charge

The induced charge signal, Q_P, is a measure of the intrinsic charge carried by a dust particle entering the dust sensor. For two reasons the induced charge measurement is the most difficult measurement of the dust instrument: (1) Cosmic dust particles are only weakly charged. A surface potential U results in a dust charge $q = 4\pi\epsilon_0 Us$ for a spherical particle with radius s ($\epsilon_0 = 8.854 \times 10^{-12}\ \mathrm{A\,s\,V^{-1}\,m^{-1}}$). For a typical potential of $U = 5$ V, the smallest particle exceeding the detection threshold has a radius of about 20 μm, or, assuming a density of $3.3 \times 10^3\ \mathrm{kg\,m^{-3}}$, a corresponding mass of about 10^{-10} kg. The majority of the particles detected during the *Ulysses* mission had masses below 10^{-12} kg (Figure 3). (2) The charge grid is the measuring channel most exposed to ambient noise. Thus, analysis of the charge measurements requires careful consideration of the noise. As a consequence, no charges have yet been determined from the *Ulysses* and *Galileo* dust data (Svestka et al. 1996).

The *Cassini* dust instrument is by an order of magnitude more sensitive in Q_P, which led to the detection of the intrinsic charges for several interplanetary particles and for particles in Saturn's E ring (Kempf et al. 2004, 2006).

2.4. Angular Sensitivity and Sensor Pointing

Ulysses was a spinning spacecraft with a period of five revolutions per minute. The spin axis was the center line of the craft's high-gain antenna, which normally pointed at Earth, and most of the time the spin axis pointing was within 1° of the nominal Earth direction for data transmission. This small deviation is usually negligible for the analysis of measurements with the dust detector. The *Ulysses* spacecraft and mission were explained in more detail by Wenzel et al. (1992).

The *Ulysses* dust sensor had a 140° wide field of view with a sensor area of $1000\,\mathrm{cm}^2$, and it was mounted on the spacecraft nearly at right angles (85°) to the antenna axis (spacecraft spin axis). As a result of this mounting geometry, the sensor was most sensitive to particles approaching from the plane perpendicular to the spacecraft-Earth direction. The detection geometry of the sensor is illustrated in Figure 1. The impact direction of dust particles was measured by the rotation angle, θ, which was the sensor viewing direction at the time of a dust impact. During one spin revolution of the spacecraft, the rotation angle scanned through a complete circle of 360°. It was measured in a right-handed system, and $\theta = 0°$ was defined to be the direction closest to ecliptic north. At $\theta = 90°$ and 270° the sensor axis pointed nearly along the ecliptic plane. When *Ulysses* was at high ecliptic latitudes, however, the sensor pointing at $\theta = 0°$ significantly deviated from the actual north direction. During the passages over the Sun's polar regions, the sensor always scanned through a plane tilted by about 30° from the ecliptic plane, and all rotation angles lay close to the ecliptic plane (Figure 1).

The geometric detection probability for dust particles is defined by the sensitivity of the detector for particles impinging from different directions in an isotropic flux of particles. Directions are defined by the impact angle, ϕ, with respect to the sensor axis. The sensitive area as a function of ϕ is basically a cosine function modified by the shielding of the detector side wall (Grün et al. 1992a). The maximum area of $0.1\ \mathrm{m}^2$ is found for $\phi = 0°$, and the sensor field of view is a cone with 70° half angle. The solid angle covered by the detector is 1.45 sr. In an isotropic flux, 50% of the particles hit the detector at $\phi < 32°$, while the impact direction of a single particle is only known to be somewhere within the 140° wide field of view. The average of all the rotation angle arrival directions of dust particles belonging to a stream is known to much higher accuracy than is the impact directon of a single particle.

Because of the mounting of the dust detector almost perpendicular to the spacecraft spin axis, the effective sensor area for dust impacts depends on the angle between the impact direction and the spin axis. The maximum sensitive area of the detector averaged over one spacecraft revolution is $0.02\,\mathrm{m}^2$ (Grün et al. 1992b).

Laboratory experiments showed that the sensor side wall was as sensitive to dust impacts as the target itself (Willis et al. 2005), and candidates for wall impactors were indeed identified in the *Ulysses* interstellar dust data (Altobelli et al. 2004). While relaxing directional constraints, the wall impactors are not likely to change our conclusions on grain sizes. The charge Q_I measured on the ion collector of the dust instrument did not significantly differ between impacts onto the target and the sensor side wall.

2.5. Dust Impact Identification

The *Ulysses* sensor implements a highly reliable coincidence scheme of impact identification. Electrical signals in three independent channels arriving from a single dust impact are measured within less than 1 ms by two different methods (two charge-sensitive amplifiers and one multiplier). The amplitude ratios, the rise times, and the coincidence times are checked with reference to values that were obtained in calibration experiments, and true impacts are separated from noise events; the latter mostly trigger only a single channel.

Each measured signal (noise event or dust impact) was classified according to the strength of its ion charge signal (Q_I) into one of six amplitude ranges. Each amplitude range corresponds to roughly one decade in electronic charge Q_I. In addition, each event was classified into one of four event classes. The event classification scheme, defining the criteria to be satisfied for each class, is given in Baguhl et al. (1993) and Krüger et al. (1999a). This classification scheme was used for a reliable separation of noise events from true dust impacts. Real dust impacts had at least two charge measurements plus additional coincidence criteria that had to be fulfilled (see Table 1).

Four classes, together with six amplitude ranges, represent 24 separate categories. Each of these categories had its own 8 bit counter. Each signal registered by the dust instrument (noise event or dust impact) was counted with one of these counters even if the complete data set of the measured impact parameters (charges, rise times, coincidences, impact direction, etc.) was not transmitted to Earth. During periods of very high dust impact rates, a small number of data sets were lost owing to the limited data transmission rate of *Ulysses* (see also Section 3). The counter values, however, were always transmitted so that impact rates could be reconstructed.

2.6. Dust Instrument Operation

The *Ulysses* dust detector was operated almost without interruption from launch in 1990 until 2001. Owing to decreasing power generation of the radioisotope batteries (RTGs), however, the available electrical power on board the spacecraft became an issue in 2001. Some instruments on board had to be switched off temporarily, and a cycling instrument operation scheme had to be implemented: one or more of the scientific instruments had to be switched off at a time. As a consequence, the dust instrument was switched off repeatedly (Grün et al. 1995a; Krüger et al. 1999a, 2001, 2006a, 2010). After 2007 November 30, the dust instrument remained switched off permanently even though the *Ulysses* spacecraft operation continued until 2009 June 30.

Degradation of the dust instrument electronics, in particular the channeltron, was continuously monitored during the mission. We observed a channeltron degradation after approximately 10 yr of operation, which was counterbalanced by an increase of the channeltron high voltage. We did not identify any other indications for instrument aging in the *Ulysses* dust data. The smooth and rather undegraded behavior of the *Ulysses* dust instrument is in contrast to the twin instrument on board *Galileo*: the electronics of the *Galileo* instrument suffered severe degradation owing to the harsh radiation environment in Jupiter's magnetosphere (Krüger et al. 2005); nevertheless, the coincidence scheme provided reliable impact identification even then.

3. IDENTIFICATION OF INTERSTELLAR DUST IMPACTORS

During the entire *Ulysses* mission, the full data sets of 6719 dust impacts (containing impact time, impact charges, charge rise times, impact direction, etc., for each dust impact; see Table 1) were successfully transmitted to Earth (Krüger et al. 2010). During most time periods when the dust detector was operated, the impact rates were sufficiently low that the data sets of all recorded impacts could be transmitted to Earth. Only around the Jupiter flybys in 1992 and 2004 were very high impact rates recorded, so that the data sets of a large fraction of the detected impacts could not be transmitted to Earth during short intervals. All impacts, however, were always counted with the particle counters of the dust instrument (see, e.g., Krüger et al. 2006a, for details). During the time intervals of interstellar dust measurements considered in this paper, the data sets of all recorded impacts were transmitted.

An analysis of the dynamical properties (flux, impact direction) of the interstellar dust grains detected during the entire *Ulysses* mission is given by Strub et al. (2015), and theoretical predictions for interstellar dust flux, flow direction, and mass distribution for *Ulysses* are studied by Sterken et al. (2015). In the present work we analyze the mass distribution of the interstellar grains as derived from the entire mission. To this end, we first have to identify the interstellar impactors in the *Ulysses* data set.

3.1. Dust Grain Dynamics

The dynamics of interstellar dust grains in the solar system is dominated by three major forces: solar gravity, solar radiation, and the Lorentz force. Here we briefly discuss the most important aspects for particle motion in the solar system; a more comprehensive discussion is given in the accompanying paper by Sterken et al. (2015).

Micrometer-sized and submicrometer-sized dust particles are susceptible to a pressure exerted by the solar radiation field. Given that the solar radiation expands with the inverse square of the heliocentric distance, r, the radiation pressure force $F_{\rm RP}$ follows the same distance dependence as solar gravity $F_{\rm grav}$ (i.e., r^{-2}). Hence, the ratio $\beta = F_{\rm RP}/F_{\rm grav}$ is constant for a given particle and depends on particle size, optical properties, morphology, etc. The radiation pressure is strongly size dependent, with a broad maximum for grain sizes approximately comparable to the wavelength of the incident radiation, i.e., for submicrometer-sized grains. For strongly absorbing materials, the β ratio can be larger than 1.

Interstellar particles with $\beta > 1$ are deflected by the solar radiation, leading to an avoidance cone close to the Sun. For $\beta = 1$ radiation pressure and gravity cancel out and the particles move on straight "undisturbed" trajectories. Particles with $\beta < 1$ are concentrated downstream from the Sun.

Dust particles in interplanetary space usually carry an electric charge due to photoionization by the solar radiation field, making them susceptible to the Lorentz force exerted by their motion through the IMF. The field strength, orientation w.r.t. the particle motion, and the particles' charge-to-mass ratio, Q/m, determine the strength of the Lorentz force. The surface charge of a spherical grain increases linearly with the grain radius, a, while the mass has an a^3 dependence. Hence, the relative strength of the Lorentz force strongly increases for smaller particles. For a more detailed discussion the reader is referred to Sterken et al. (2015).

For the conditions in interplanetary space the Lorentz force becomes the dominating force for particles smaller than approximately $a \lesssim 0.1\,\mu$m (Landgraf 1998, his Figure 3.5; note that this value strongly depends on heliocentric distance). Particles larger than approximately 1 μm have a low charge-to-mass ratio and low β, and their dynamics is dominated by gravity. In the intermediate size range, radiation pressure makes a significant contribution, and it may even become the dominant force between 0.1 and 0.4 μm (Kimura & Mann 1999).

The Lorentz force depends on the 22 yr solar (magnetic) cycle, leading to a focusing and defocusing configuration for interstellar dust. Particles with sufficiently high Q/m are likely not able to penetrate the heliopause (Linde & Gombosi 2000 note that these authors studied only the defocusing phase of the solar cycle).

We ignore the Poynting–Robertson drag force, which is due to an abberation effect exerted on dust grains by the solar radiation field. It causes approximately micrometer-sized particles initially orbiting the Sun at 1 AU distance to spiral into the Sun on timescales of 10^3–10^4 yr. The interstellar grains traverse the solar system within 20–50 yr, and they spend a much shorter time close to the Sun where the Poynting–Robertson drag is strongest. The resulting grain deflection is very small and thus negligible in our case.

We ignore any rotation of the dust grains that might lead to rotational bursting of the grains. Rotational bursting, which might have an effect on the dust mass distribution by creating an excess of small grains, is not expected for interstellar grains in the heliosphere (Misconi 1993; Draine 2011). Similarly, the Yarkovsky effect can be ignored for the interstellar dust grains (Gustafson 1994).

Furthermore, one might expect a contribution from the rotational energy of the grains to the energy released during impact onto the detector target. The rotational energy of micrometer- and submicrometer-sized grains is 10–15 orders of magnitude smaller than the kinetic energy of the grains. Hence, the rotational energy can be completely ignored for the calibration of our impact measurements. We also ignore any other mechanisms of grain destruction (see Frisch et al. 1999, their Section 4.4).

3.2. Grain Selection Criteria

The *Ulysses* dust data contain impacts by interplanetary and interstellar grains. Therefore, we have to find selection criteria that allow us to define data sets with a negligible number of impacts from sources other than interstellar. For the identification of the interstellar impactors we have adopted the same selection criteria as Landgraf (1998) and Frisch et al. (1999) and applied them to the entire *Ulysses* mission. These criteria were based on the following observations that we are reviewing here:

1. After its Jupiter flyby in 1992 February, *Ulysses* observed a relatively constant flux of dust particles above and below the ecliptic plane. The approach direction of these grains was opposite to the direction of interplanetary dust during most of the time, except around *Ulysses*'s perihelion. Hence, they appeared to be in retrograde motion about the Sun (Figure 1). If we assume that these grains enter the solar system from close to the upstream direction of the interstellar helium gas as observed by *Ulysses*, their impact direction is compatible with an origin from outside the solar system.
2. Applying the mass and speed calibration of the dust instrument, most particles had impact speeds in excess of the solar system escape speed, also pointing to an origin from outside the solar system.

3. The flux of the interstellar particles was independent of ecliptic latitude (Landgraf et al. 2003; Krüger et al. 2007), in contrast to interplanetary dust that is strongly concentrated toward the ecliptic plane and the inner solar system. Dust emanating from the Jovian system is concentrated in the vicinity of Jupiter (Grün et al. 1993; Krüger et al. 2006b).

From the above observations we derive the following identification criteria for interstellar grains: from observation 1 we select every impact that was measured when the interstellar helium flow direction was within the $\pm 70°$ field of view of the dust detector. We add a $20°$ margin because the sensor side wall turned out to be as sensitive to dust impacts as the target itself (Section 2.4). When *Ulysses* crossed the ecliptic plane at a heliocentric distance of about 1.3 AU, the impact directions of interstellar and prograde interplanetary grains were not as clearly separated as was the case during the rest of the *Ulysses* orbit. We therefore exlude all impacts around perihelion when *Ulysses* was between $-60°$ and $+60°$ ecliptic latitude.

Over the poles of the Sun, *Ulysses* detected very small particles, which were interpreted as fragments of interplanetary grains ejected from the inner solar system by electromagnetic effects (Hamilton et al. 1996) and solar radiation pressure (Wehry & Mann 1999; Wehry et al. 2004). In order to remove these particles from the data set, the measured amplitude of the ion charge signal, Q_I, had to be more than one order of magnitude above the detection threshold of the dust instrument. Therefore, over the poles of the Sun, at ecliptic latitudes $|b| \geqslant 60°$, we ignore impacts with impact charge amplitudes $Q_I \leqslant 10^{-13}$ C.

Around the Jupiter flybys in 1992 and 2004 *Ulysses* detected collimated streams of dust particles originating from within Jupiter's magnetosphere (Grün et al. 1993). In order to avoid contamination of the interstellar dust data set, the measurements during the periods of identified Jovian dust streams were ignored entirely. The times when the dust streams occurred were given by Baguhl et al. (1993) and Krüger et al. (2006b) and are adopted here.

Finally, a shift in the approach direction of the interstellar grains by about $40°$ was recognized in 2005 and 2006 (Krüger et al. 2007; Strub et al. 2011, 2015). Therefore, in 2005/2006 the nominal band of rotation angles of $\pm 90°$ within the interstellar helium flow direction was expanded toward larger rotation angles by $40°$ to take this shift into account (see Figure 4).

The selection criteria for the identification of interstellar grains are listed in Table 2. Our criteria are different from those adopted by Strub et al. (2015). Since our aim is to derive the mass distribution of the grains, we have to use criteria that do not induce any bias in the mass distribution. Therefore, we did not constrain the measured impact charge, Q_I, except for short periods over the poles of the Sun (see Table 2). We used the observed impact direction of the interstellar grains by constraining the rotation angle. We do not expect to introduce a bias in the mass distribution this way. On the other hand, Strub et al. (2015) analyze the dynamical properties of the grains. For example, to avoid any bias in the measured impact directions, these authors did not constrain the rotation angle.

After removing potential impacts by interplanetary particles with the method described above, we identified 987 interstellar grains in the *Ulysses* data (compared to 526 interstellar grains identified by Strub et al. 2015). The *Ulysses* interstellar dust data are shown in Figure 4 (subsets of the *Ulysses* interstellar dust data for different size bins are shown in Figure 8 in the Appendix). This extends the number of detected interstellar grains by more than a factor of three compared to earlier analyses (305 *Ulysses* impacts between Jupiter flyby in 1992 February and 1996 March; Landgraf 1998; Frisch et al. 1999).

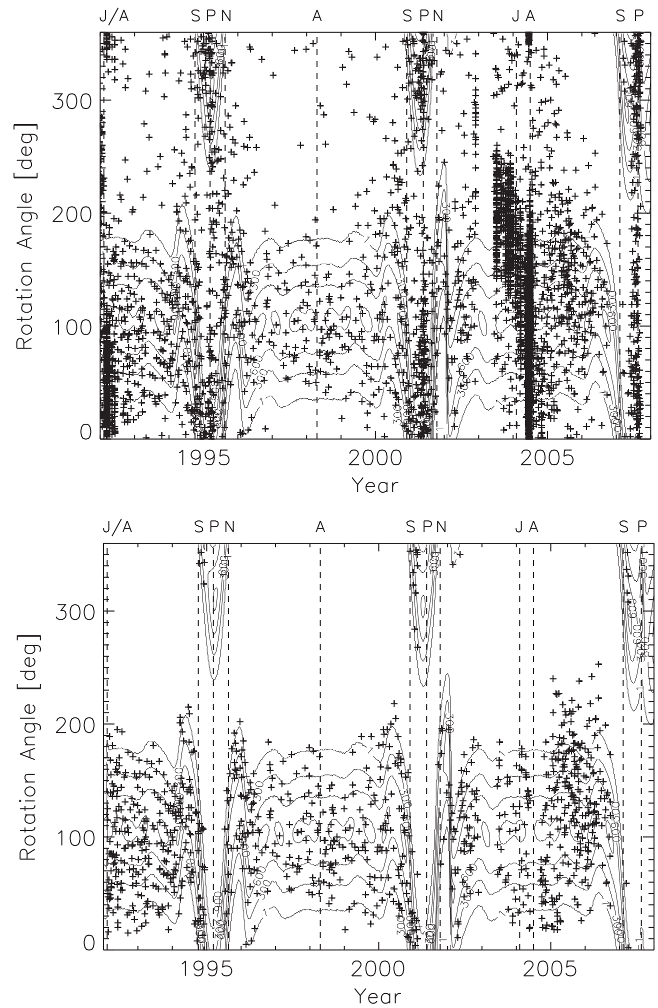

Figure 4. Impact direction (rotation angle) vs. time for all dust impacts detected between Jupiter flyby in 1992 February and the end of dust instrument operation in 2007 November (top) and for the identified interstellar dust impactors (bottom). Each plus sign indicates an individual dust particle impact. Contour lines show the effective sensor area for dust particles approaching from the upstream direction of interstellar helium (McComas et al. 2012). Vertical dashed lines and labels at the top indicate *Ulysses*'s Jupiter flybys (J), perihelion passages (P), aphelion passages (A), south polar passes (S), and north polar passes of *Ulysses* (N).

The earlier works also considered 309 interstellar dust impacts measured with *Galileo*. Here we use only the *Ulysses* data. Inclusion of the *Galileo* data would extend the entire data set by only approximately 1/3 and, hence, not seriously increase the statistical significance of our results. On the other hand, Landgraf et al. (2000) concluded that the *Galileo* data set is likely contaminated with impacts by interplanetary grains. *Galileo* measured only in the ecliptic plane, where a stronger contribution by interplanetary impactors has to be expected, while *Ulysses* measured out of the ecliptic plane most of the time.

Table 2
Criteria for the Identification of Interstellar Dust Grains Used in This Paper

Criteria	Time Period/ Spatial Region	Comments
Rotation angle within ±90° of interstellar helium flow direction	Entire data set	Sensor target plus side wall
Rotation angle within ±90° of interstellar helium flow direction plus 40° toward positive rotation angles	2005/2006	Observed shift in rotation angle
$Q_I > 10^{-13}$ C for impacts at ecliptic latitude $\|b\| \geqslant 60°$	Sun's polar regions	Removal of electromagnetically accelerated grains
All dust impacts ignored with $\|b\| < 60°$ around perihelion	Inner solar system	No separation from interplanetary impactors possible
All dust impacts ignored in 39 short time intervals defined by Baguhl et al. (1993) and Krüger et al. (2006b)	1992/1993 and 2002–2005	Jupiter dust streams removal

3.3. Dust Impact Speed

The grain impact speed derived from the instrument calibration can be considered as an independent consistency check of our grain selection criteria. Out of the data set of 987 interstellar grains identified by the selection criteria described in Section 3.2, we selected only those grains with a reliable measurement of the charge rise times, t_I and t_E, and, hence, a reliable determination of the grain impact speed (i.e., velocity error factor VEF < 6; Krüger et al. 2010). This results in a data set of 943 particles. The average impact speed of these grains is $24 \pm 12\ \mathrm{km\ s^{-1}}$, confirming earlier results by Kimura et al. (2003a). Even though this value is very close to the measured speed of the interstellar gas of 23–26 $\mathrm{km\ s^{-1}}$, it should not be taken as a discriminator for either of the two values owing to the factor of two uncertainty in the measurement of the interstellar dust speed.

From modeling the particle dynamics (e.g., Sterken et al. 2015) the largest grains are expected to have the highest impact speed owing to gravitational acceleration, the midsized particles with sizes close to the maximum of the β curve have smaller impact speeds, and the smallest particles have variable speeds owing to the Lorentz force. The measured average impact speed is in agreement with our hypothesis that the interstellar dust flow is generally coupled with the gas, and that the majority of the grains in our selected data set are indeed of interstellar origin.

3.4. Determining the Dust Mass Distribution

The most straightforward determination of the grain mass is based on the laboratory calibration of the dust instrument and relies on the grain impact speed as derived from the measured rise time of the charge signal (see Section 2.3). Equation (1) shows that the mass obtained from the impact charge measurement has a strong dependence on the impact speed, with a power-law index of approximately 3.5. Given that the speed calibration has a factor of two uncertainty, this yields a factor of 10 uncertainty in the derived mass.

A more accurate mass can be derived if the grain impact speed is known by other means. Such a technique was successfully applied earlier to *Ulysses* interstellar dust measurements by Landgraf et al. (2000) and to *Galileo* dust measurements of grains ejected from the Galilean moons (Krüger et al. 2000, 2003). In the present work we apply two similar approaches to determine the impact speed of the interstellar dust grains. Both take into account the change in velocity of an interstellar grain in the heliosphere, which can—in principle—easily be determined from the acceleration due to solar gravity and radiation pressure. We neglect the Lorentz force exerted on the grains by interaction with the solar wind magnetic field, which is a good approximation for grains more massive than approximately 10^{-16} kg. The Larmor radii for such particles are on the order of 500 AU in the region traversed by *Ulysses*, increasing with distance from the Sun (Grün et al. 1994). They are much larger than the length of their interaction with the solar wind.

The relative strength of radiation pressure is expressed as the ratio, β, between the radiation pressure force and the gravitational force (Section 3.1). For submicrometer-sized grains radiation pressure can be of the same order ($\beta \approx 1$) or even larger than gravity ($\beta > 1$). We therefore consider two simple cases, following the strategy applied by Landgraf et al. (2000):

- **Model 1:** The radiation pressure force and gravity acting on a dust grain have exactly the same strength but opposite directions ($\beta = 1$, fixed). Therefore, the interstellar grains move through the solar system on straight lines. Their velocity and flow direction remain unchanged. In this case, the impact velocity is given by the difference between the grain velocity at infinity and the spacecraft velocity.
- **Model 2:** The ratio β depends on the grain size. In this case, the grain velocity is affected by radiation pressure and gravity. We calculate β and the grain velocity for each grain individually. We take β from Kimura & Mann (1999) as a function of grain radius, a, for compact spherical grains made of astronomical silicates, having a bulk density of $\rho = 3.3 \times 10^3\ \mathrm{kg\ m^{-3}}$. The grain radius, however, is not measured independently by the dust instrument. We therefore have to derive the radius from the grain mass, m, obtained from the impact charge measurement. The radius of a spherical grain is given by $a = (3\,m/(4\pi\rho))^{\frac{1}{3}}$. Using the grain radius, we can

determine the dust velocity in the heliocentric frame and hence the impact velocity onto the sensor target. Then, an improved grain mass can be calculated by inversion of Equation (1). From this mass we determine a new grain radius, which gives us a new β, and so forth. This iterative process leads to a value of β in a self-consistent way.

A disadvantage of this second method is its dependence on the detailed properties of the dust grains, which are not well known. We therefore apply both models and compare the results. It turned out that $\beta = 1$ is a good approximation for the majority of the impacts detected with *Ulysses* and *Galileo* (Landgraf et al. 2000). For the biggest detected grains and for the smallest ones, however, this is not a good approximation. Here, the second model is expected to give better results.

For both models we assume an initial velocity of the grains outside the heliosphere of 23.2 km s^{-1} (McComas et al. 2012). This value is about 10% smaller than the value of 26 km s^{-1} that was earlier adopted by Landgraf et al. (2000). Equation (1) shows that the derived grain masses increase by about 50% as a result of this reduced impact speed.

We assume an upstream direction of the interstellar dust flow of 250° ecliptic longitude and 8° latitude as was recently derived by Strub et al. (2015). The longitude is somewhat smaller than the value derived by Landgraf (1998; 259°). Given the large field of view of the dust detector, this is well within the measurement uncertainty. For most of the time, except in 2005/2006, this initial velocity vector is (1) compatible with the heliocentric speed and the direction of motion of the interstellar grains detected with *Ulysses* (Grün et al. 1994; Baguhl et al. 1995b), (2) close to the asymptotic velocity vector of the interstellar helium flow detected by *Ulysses* and *IBEX* (Witte 2004; McComas et al. 2012; Section 1), and (3) close to the velocity of the Sun with respect to the LIC (Lallement & Bertin 1992). In 2005/2006 we take a 40° shift in the grain impact direction into account (Strub et al. 2015).

A recent analysis of neutral helium measurements revealed a potential temporal variation of the inflow direction and speed of neutral helium over four decades (Frisch et al. 2013), which was later put into question by Lallement & Bertaux (2014), who found no evidence for such a variation. For the measurement period of the *Ulysses* interstellar dust measurements this corresponds to a shift of 2.°7 over 16 yr. Given the large field of view of the dust detector (Section 2.4), this value is negligible for our analysis.

4. RESULTS

4.1. Dust Mass Distribution

The resulting mass distributions for the three cases considered (calibrated impact speed, $\beta = 1$ [model 1], and β variable self-consistent [model 2]) are shown in Figure 5. They cover a mass range from approximately 10^{-18} kg (which is the detection threshold for grains impacting with 20 km s^{-1}) to 10^{-10} kg with maxima at about 10^{-17}–10^{-16} kg. From modeling the extinction of starlight (Mathis et al. 1977; Draine 2009) it is expected that the number of grains per mass interval steeply rises toward smaller grain masses. This is not seen in the in situ data; instead, the mass distribution shows a deficiency of small grains below approximately 10^{-16} kg (top panel). This deficiency is most likely due to the interaction of the grains with the IMF (Grün et al. 1994). The upper mass limit at approximately 10^{-11} kg is determined by the size of the

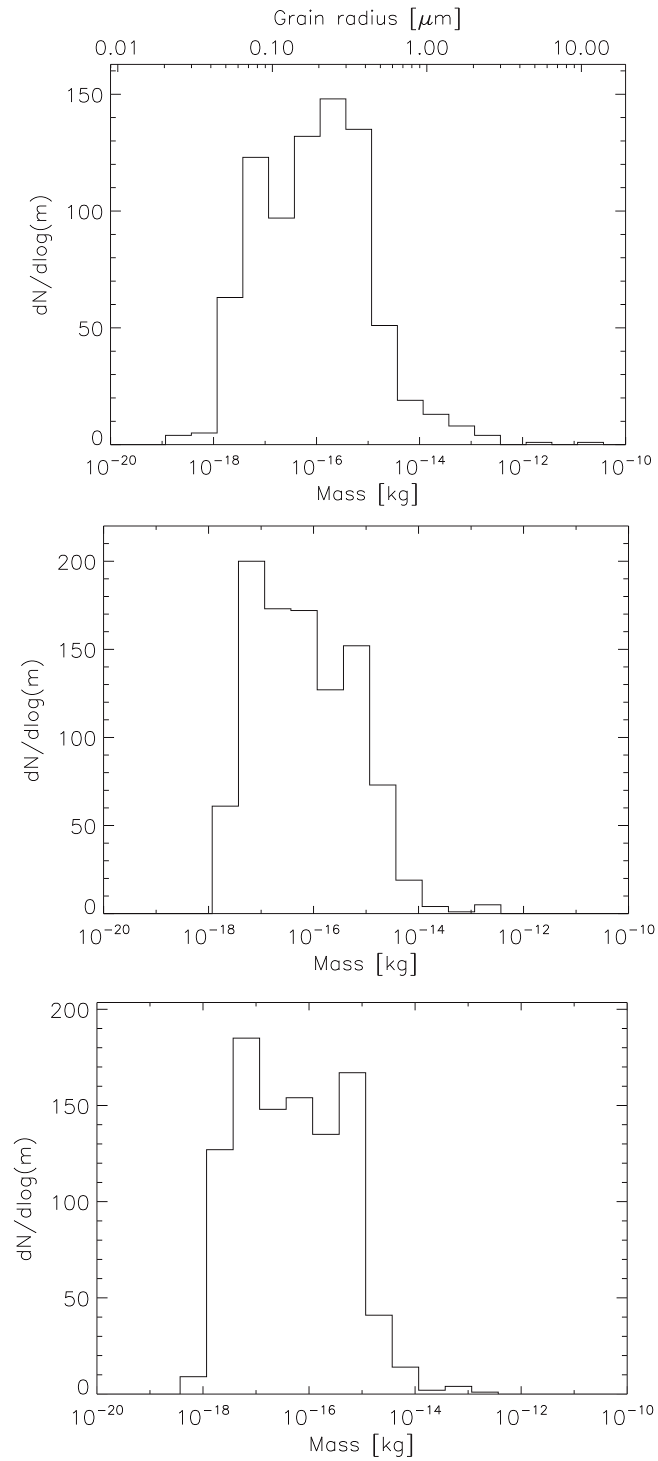

Figure 5. Mass distribution of interstellar grains derived from the *Ulysses* measurements shown as number of particles per logarithmic mass interval for three different cases for the impact speed calculation. Top panel: grain masses derived from the measured impact speeds. Only particles with impact speed $v > 13$ km s^{-1} were considered (804 particles). Middle panel: masses derived from the $\beta = 1$ model, taking into account the spacecraft motion (model 1). Bottom panel: masses derived self-consistently (model 2) with accelerated ($\beta < 1$) and decelerated ($\beta > 1$) grains (987 particles for both models). The approximate grain size for spherical particles with density $\rho = 3.3 \times 10^3$ kg m^{-3} is shown at the top for comparison.

dust detector: large grains are much less abundant than small ones, so that only very few large grains were detected.

Comparison of the top panel with the two lower panels in Figure 5 shows that the proportion of particles below 10^{-16} kg is

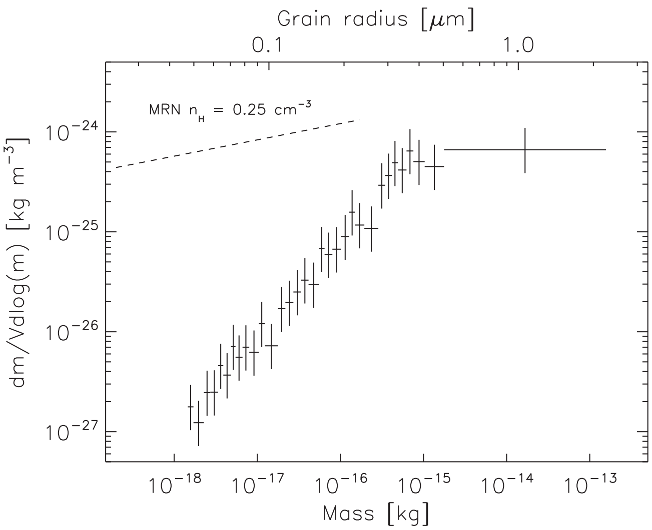

Figure 6. Mass distribution of interstellar grains derived from the *Ulysses* measurements shown as mass per logarithmic mass interval and unit volume (987 particles). The approximate grain size for spherical particles with density $\rho = 3.3 \times 10^3$ kg m^{-3} is shown at the top for comparison. The dashed line shows the mass distribution derived from astronomical observations (Mathis et al. 1977) for an interstellar hydrogen density of 0.25 cm $^{-3}$. Grain masses were derived from the self-consistent model with accelerated ($\beta < 1$) and decelerated ($\beta > 1$) grains. The data are tabulated in Table 3.

increased and the fraction of particles above this limit is reduced when we derive the grain masses from the $\beta = 1$ model and the self-consistent model for the grain impact speed. A similar result was also found by Landgraf et al. (2000) from the analysis of the *Galileo* and the smaller *Ulysses* interstellar dust data sets available at the time. It was explained either by being due to a contamination by interplanetary impactors that might have lower impact speeds than the interstellar grains or by recombination in the impact-generated plasma cloud in the detector.

The mass distributions derived from the two impact speed models ($\beta = 1$ and the self-consistent model) are very similar, except that the number of grains at the high-mass end is even further reduced in the self-consistent model (see middle and bottom panels of Figure 5), again confirming earlier results by Landgraf et al. (2000).

We now consider the contributions of grains with different masses to the overall mass density of interstellar dust in the solar system. In Figure 6 we show the mass distribution of interstellar grains as the differential mass density per unit volume (987 particles; see also Frisch et al. 1999). The distribution derived from astronomical observations (Mathis et al. 1977, hereafter MRN) for an interstellar hydrogen density of 0.22 cm^{-3} is shown for comparison. Particles with masses below approximately 10^{-16} kg are strongly depleted in the inner heliosphere owing to heliospheric filtering, as compared to the ISM. For instance, the density of grains with mass 10^{-17} kg is reduced in the inner heliosphere by about a factor of 90 below the MRN prediction, while 10^{-18} kg grains are deficient by three orders of magnitude. At the same time large (approximately 10^{-14} kg) grains are absent in the MRN distribution but are abundant in the inflowing interstellar dust. It is incompatible with both interstellar elemental abundances and the observed extinction properties of the interstellar dust population (Draine 2009). The solar system may by chance be located near a concentration of massive grains in the ISM ($\ll$1 kpc; Grün & Landgraf 2000).

The existence of interstellar grains larger than approximately 10^{-16} kg as derived from the *Ulysses* and *Galileo* data was an important result from the earlier interstellar dust measurements. The largest contribution of the detected grains to the optical cross section is provided by grains in the range from 10^{-16} to 10^{-14} kg, while smaller grains below 10^{-16} kg that are believed to dominate the extinction of starlight do not contribute much to the mass density (Landgraf et al. 2000). Such small grains are significantly depleted in the *Ulysses* data owing to interaction with the IMF and the heliospheric boundary during certain time intervals (Slavin & Frisch 2008; Slavin et al. 2010). On the other hand, the large grains above 10^{-16} kg provide a significant contribution to the total mass of dust in the ISM, given their large masses and relative abundance.

The total mass density of interstellar grains as derived from the *Ulysses* in situ data can be obtained by integrating over the differential distribution shown in Figure 6. This yields a total mass density of $(2.1 \pm 0.6) \times 10^{-24}$ kg m^{-3}, which is a factor of three smaller than the value derived by Landgraf et al. (2000). This value is dominated by the largest particles detected (see Landgraf et al. 2000, their Figure 7(c)). The reduced dust density reflects a smaller proportion of the biggest grains detected after 2000, assuming that there are no small-scale variations in the dust density in the ambient ISM close to our solar system. Temporal variations in the flux of these large grains are not likely, as they are only marginally affected by the time-variable IMF. On the other hand, the dust density varies spatially as the large grains are focused in the downstream direction behind the Sun. When *Ulysses* moved toward the Sun, a dust density increase by a factor of 1–1.5 and a relative increase in interstellar flux by a factor of 2–2.5 with respect to the undisturbed incoming density and flux are expected from simulations (Sterken et al. 2015). However, these regions around *Ulysses*'s perihelion are ignored in the data selection, so that this has a minor effect on the derived mass distribution.

4.2. Gas-to-dust Mass Ratio in the Local Interstellar Cloud

From the total mass density derived from the in situ measurements we can calculate the gas-to-dust mass ratio in the LIC surrounding our solar system. This gives us information about the refractory elements in our local interstellar environment. We adopt a recently determined total hydrogen density of $n_{\rm H} = 0.247$ cm^{-3} (i.e., neutral hydrogen density $n_{\rm HI} = 0.192$ cm^{-3} and proton density $n_{\rm p} = 0.0554$ cm^{-3}; Slavin & Frisch 2008, their model 26) and a neutral helium density of $n_{\rm He} = 0.015$ cm^{-3} (Möbius et al. 2004). Using the total dust mass density derived from the interstellar grains detected with *Ulysses* (Section 3.4), we find a gas-to-dust mass ratio in the LIC of $R_{\rm g/d} = 193^{+85}_{-57}$. This value is somewhat higher than the dust density derived from earlier investigations ($R_{\rm g/d} \sim 94$–127; Frisch et al. 1999; Landgraf et al. 2000; Kimura et al. 2003a; Altobelli et al. 2004). It should be mentioned that there is some uncertainty in the total hydrogen density. For example, Heerikhuisen & Pogorelov (2011), from heliosphere models, find a somewhat lower value of $n_{\rm H} = 0.21$–0.23 cm^{-3}. In our analysis, a value of $n_{\rm H} = 0.22$ cm^{-3} results in $R_{\rm g/d} = 172$.

Gas-to-dust mass ratios calculated from more recent models with improved solar abundances are in the range $R_{\rm g/d} \sim 149$–217 (Slavin & Frisch 2008). Thus, our present analysis is in good agreement with the results obtained from astronomical observations.

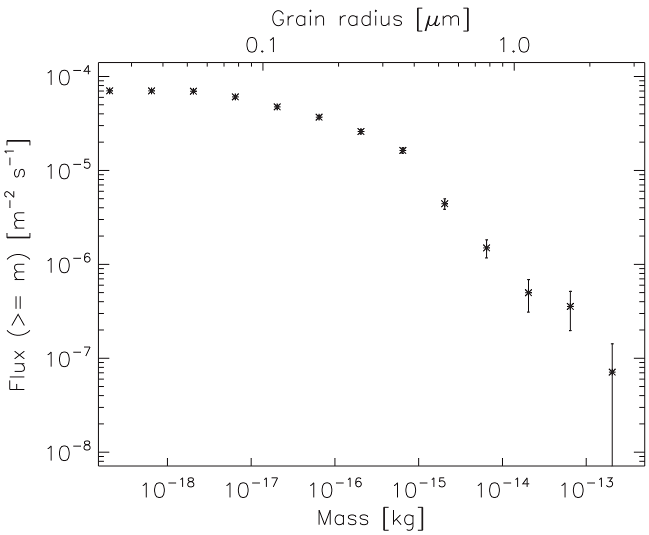

Figure 7. Flux of interstellar grains derived from the *Ulysses* measurements with the self-consistent model with accelerated ($\beta < 1$) and decelerated ($\beta > 1$) grains. The approximate grain size for spherical particles with density $\rho = 3.3 \times 10^3\ \mathrm{kg\ m^{-3}}$ is shown at the top for comparison. The data are tabulated in Table 4.

4.3. Interstellar Dust Flux

In Figure 7 we show the cumulative mass flux as derived from the *Ulysses* interstellar dust measurements. Here we show only the self-consistent model for the speed calibration (model 2). For a discussion of the two other alternatives for calibrating the grain masses the reader is referred to Landgraf et al. (2000). The dust flux distribution extends to somewhat larger particles as compared to the earlier analysis by Landgraf et al. (2000) for two reasons: (1) the reduced impact speed in our present analysis leads to larger grain masses, and (2) the dust data set contains about a factor of three more particles, so that the dust detector had a higher chance to catch larger particles. The flux of 10^{-13} kg particles is on the order of $10^{-7}\ \mathrm{m^{-2}\ s^{-1}}$.

5. DISCUSSION

The *Stardust* mission recently returned samples of contemporary interstellar grains to Earth. Preliminary analysis of a few of these grains extracted from the interstellar collector indicates that their bulk density is rather low (Westphal et al. 2014). In addition, Sterken et al. (2015) derive a low-density of interstellar dust from their simulations in the context of *Ulysses* observations. The bulk density affects the charge-to-mass ratio for a given size and, hence, the grain interaction with the IMF.

In our analysis we assumed the grains to be compact, spherical, and composed of astronomical silicates with density $\rho = 3.3 \times 10^3\ \mathrm{kg\ m^{-3}}$ (Kimura & Mann 1999). We did not consider porous grains for three reasons: (1) The bulk density is not yet well established from the analysis of the *Stardust* samples. (2) The laboratory calibration of the *Ulysses* dust detector was performed solely with compact grains; only recently are there attempts to calibrate the dust detector with low-density grains with the Heidelberg Dust Accelerator (Sterken et al. 2013b). (3) Finally, the β curves for porous particles are currently under review (H. Kimura 2015, private communication). Once these prerequisites are fulfilled, it will be possible to do the next major step in deriving a more consistent calibration of the interstellar grain mass distribution, matching also the *Stardust* results. We estimate that if the interstellar grains are indeed of low density, their masses will be typically overestimated by one order of magnitude in the *Ulysses* data (Hornung 2012, personal communication; Sterken 2012; Sterken et al. 2015), but this still needs experimental proof. This would increase the gas-to-dust ratio calculated in this paper. On the other hand, many big particles, the flux of which peaks around perihelion (Sterken et al. 2015), were left out of the selection (Section 3). This could reduce the gas-to-dust mass ratio. It is not clear at this stage which effect is bigger, and this needs further investigations.

In addition to the well-recognized silicate component of interstellar dust, astronomical observations also indicate the existence of carbon grains in interstellar space (Kimura et al. 2003b; Draine 2011). Carbon has a higher albedo (i.e., higher β) than silicates and is thus more susceptible to radiation pressure. In order to test the influence of a significant carbon component in our *Ulysses* detections, we assumed that all detected grains are composed of carbon, and we used the β curves for compact carbon from Kimura & Mann (1999, their Figure 1), instead of the silicate data. With this assumption we recalculated the grain masses with our self-consistent model with variable β. This leads to a reduction in the gas-to-dust mass ratio by about 20%. It should be noted, however, that this is a very simple approach that takes into account neither the influence of the grain composition on the calibration of the impact measurements nor porosity of the grains. Furthermore, we do not know the abundance of carbon grains in the interstellar dust flow yet. The existence of the 9.7 and 18 μm infrared features observed in interstellar clouds indicates that silicate grains are abundant in interstellar space, which is also consistent with the *Stardust* results (Westphal et al. 2014).

Similarly, the entry speed of the interstellar helium into the heliosphere *was* under debate (Lallement & Bertaux 2014; McComas et al. 2015; Wood et al. 2015). Values of 23.2 and 26 $\mathrm{km\ s^{-1}}$, respectively, *were* considered. Our model, with variable β and an entry speed of the interstellar grains set to the latter value with all parameters unchanged, yields a gas-to-dust mass ratio about 20% higher than derived for the lower entry speed.

Modeling of the interaction of the small interstellar grains with the solar wind magnetic field suggests that the mass distribution changes with time (Landgraf et al. 1999, 2003; Sterken et al. 2013a). Small grains are depleted between mid-1996 and 1999 because of the defocusing configuration of the solar wind magnetic field. The analysis of the *Ulysses* data suggests such a depletion of the interstellar grains in this time interval. On the other hand, a concentration of big grains is expected in the downstream direction of the interstellar dust flow behind the Sun. Thus, the measured flux of big grains should have increased around *Ulysses*'s perihelion passage when the spacecraft was close to this region. We have ignored this time interval in our analysis because interstellar grains cannot be clearly separated from interplanetary impactors in this period.

We did not consider temporal changes in our analysis of the grain size distribution. Changes in the slope of the mass distribution are discussed in an accompanying paper by Strub et al. (2015), which revealed temporal and grain-size-dependent variations of the measured dust flux and impact direction. Simulations of the dust size and mass distributions for so-called adapted astronomical silicates show some features similar to the observed dust distribution (Sterken et al. 2015).

Dust measurements between 0.3 and 3 AU in the ecliptic plane exist also from *Helios*, *Galileo*, and *Cassini*. These data show evidence for distance-dependent alteration of the interstellar dust stream caused by solar radiation pressure, gravitational focusing by the Sun, and electromagnetic interaction of the grains with the time-varying IMF (Altobelli et al. 2003, 2005).

The gas-to-dust mass ratio derived from our analysis is dominated by the largest grains detected. The largest grains, however, are not seriously affected by radiation pressure and electromagnetic forces. The neglect of potentially big interstellar impactors in the inner solar system may lead to an overestimation of the gas-to-dust mass ratio $R_{g/d}$.

6. CONCLUSIONS

We analyzed the mass distribution of interstellar dust grains entering the heliosphere from 16 yr of *Ulysses* in situ dust measurements obtained between 1992 February and 2007 November. Our analysis extends the time period sampling the interstellar dust size distribution in the heliosphere by more than a factor of two compared to previous investigations by Landgraf et al. (2000). A total number of 987 interstellar dust impacts was identified in the *Ulysses* dust data, thus extending the total interstellar dust data set by a factor of three compared to earlier analyses.

We used a very similar technique to that of Landgraf et al. (2000), but with updated properties of the ISM: interstellar dust speed outside the heliosphere of 23.2 km s^{-1} (currently under discussion; Lallement & Bertaux 2014), total interstellar hydrogen density of 0.247 cm^{-3}, and improved ratios of radiation pressure over gravity β for astronomical silicates. We calculated the grain-size-dependent variation of the impact speed and impact direction using the dependence of radiation pressure on particle size from Kimura & Mann (1999), assuming that the grains are composed of astronomical silicates.

Our results confirm the existence of interstellar grains in the heliosphere in the size range from 0.05 μm to above 1 μm. The overall size distribution measured in situ with *Ulysses* within 5 AU from the Sun shows a deficiency of small grains below 0.3 μm, compared to astronomically observed interstellar dust in the ISM (Mathis 2000; Draine 2003; Frisch & Slavin 2013). This deficiency can be partially explained by strong heliospheric filtering (Slavin et al. 2012; Sterken et al. 2013a). Up to now, no exact fit between the simulations and the data has proven this, but the general trend can be recognized.

We find a gas-to-dust mass ratio $R_{g/d} = 193^{+85}_{-57}$. This value is compatible with gas-to-dust mass ratios derived from observations of sightlines to stars. Our analysis confirms earlier results that "big" (i.e., $\approx$1 μm sized) interstellar grains exist in the very local ISM that are not easily accessible to astronomical observations (Wang et al. 2014).

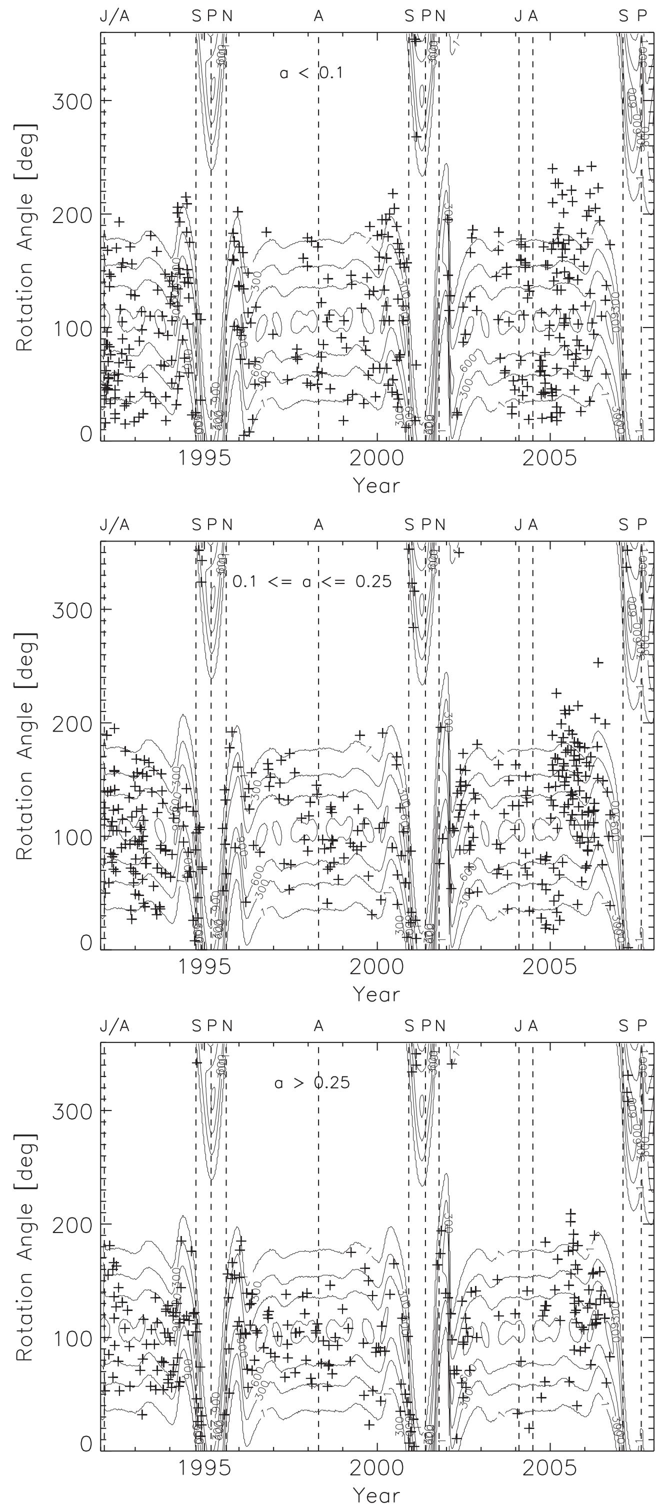

Figure 8. Same as Figure 4, but for different subsets of the interstellar dust data (assuming a grain density of 3.3 kg m^{-3}). Top: particles with radius $a < 0.1$ μm (363 particles); middle: 0.1 μm $\leqslant a \leqslant$ 0.25 μm (362 particles); bottom: $a > 0.25$ μm (262 particles).

We thank the *Ulysses* project at ESA and NASA/JPL for effective and successful mission operations and an anonymous referee for improving the presentation of our results. H.K. is also grateful to Klaus Hornung for valuable discussions during the preparation of this manuscript. This research was supported by the German Bundesministerium für Bildung und Forschung through Deutsches Zentrum für Luft-und Raumfahrt e.V. (DLR, grant 50 QN 9107). H.K. and P.S. gratefully acknowledge support by MPI für Sonnensystemforschung. P.S. acknowledges support by Deutsche Forschungsgemeinschaft (DFG) grant KR 3621/1-1.

Facility: Ulysses.

Table 3
Mass Distribution of Interstellar Grains Derived in This Paper

Mass (kg) (1)	$dm/V d\log(m)$ (kg m^{-3}) (2)	Err X+ (kg m^{-3}) (3)	Err X− (kg m^{-3}) (4)	Err Y+ (kg m^{-3}) (5)	Err Y− (kg m^{-3}) (6)
1.67E-14	6.62E-25	1.57E-13	1.77E-15	1.10E-24	3.87E-25
1.35E-15	4.50E-25	1.77E-15	1.03E-15	7.44E-25	2.63E-25
8.84E-16	5.04E-25	1.03E-15	7.56E-16	8.34E-25	2.94E-25
6.87E-16	6.45E-25	7.56E-16	6.25E-16	1.07E-24	3.76E-25
5.55E-16	4.16E-25	6.25E-16	4.92E-16	6.88E-25	2.43E-25
4.53E-16	4.91E-25	4.92E-16	4.18E-16	8.13E-25	2.87E-25
3.81E-16	3.66E-25	4.18E-16	3.47E-16	6.07E-25	2.14E-25
3.15E-16	2.93E-25	3.47E-16	2.86E-16	4.85E-25	1.71E-25
2.36E-16	1.08E-25	2.86E-16	1.94E-16	1.80E-25	6.33E-26
1.71E-16	1.17E-25	1.94E-16	1.50E-16	1.94E-25	6.83E-26
1.38E-16	1.57E-25	1.50E-16	1.28E-16	2.61E-25	9.19E-26
1.14E-16	8.94E-26	1.28E-16	1.02E-16	1.48E-25	5.22E-26
9.04E-17	6.71E-26	1.02E-16	8.01E-17	1.11E-25	3.91E-26
7.19E-17	5.94E-26	8.01E-17	6.45E-17	9.83E-26	3.47E-26
5.97E-17	6.78E-26	6.45E-17	5.52E-17	1.12E-25	3.96E-26
4.78E-17	2.97E-26	5.52E-17	4.14E-17	4.92E-26	1.74E-26
3.74E-17	3.29E-26	4.14E-17	3.38E-17	5.44E-26	1.92E-26
3.03E-17	2.50E-26	3.38E-17	2.72E-17	4.14E-26	1.46E-26
2.44E-17	1.96E-26	2.72E-17	2.18E-17	3.24E-26	1.14E-26
1.97E-17	1.70E-26	2.18E-17	1.77E-17	2.82E-26	9.93E-27
1.48E-17	7.24E-27	1.77E-17	1.23E-17	1.20E-26	4.22E-27
1.13E-17	1.20E-26	1.23E-17	1.04E-17	1.99E-26	7.03E-27
9.14E-18	6.22E-27	1.04E-17	8.01E-18	1.03E-26	3.63E-27
7.30E-18	7.01E-27	8.01E-18	6.65E-18	1.16E-26	4.09E-27
6.04E-18	5.55E-27	6.65E-18	5.48E-18	9.19E-27	3.24E-27
5.14E-18	7.11E-27	5.48E-18	4.82E-18	1.18E-26	4.15E-27
4.34E-18	3.68E-27	4.82E-18	3.90E-18	6.10E-27	2.15E-27
3.64E-18	4.58E-27	3.90E-18	3.39E-18	7.58E-27	2.67E-27
3.04E-18	2.49E-27	3.39E-18	2.72E-18	4.12E-27	1.45E-27
2.49E-18	2.46E-27	2.72E-18	2.28E-18	4.08E-27	1.44E-27
1.97E-18	1.23E-27	2.28E-18	1.71E-18	2.04E-27	7.18E-28
1.58E-18	1.77E-27	1.71E-18	1.46E-18	2.94E-27	1.04E-27
9.41E-19	1.95E-28	1.45E-18	6.12E-19	3.23E-28	1.14E-28

Note. The data are shown in Figure 6. Column (1) lists the grain mass, Column (2) lists the mass per logarithmic mass interval and unit volume, Columns (3) and (4) give mass interval used for data binning (30 particles per mass bin), and Columns (5) and (6) list the $\sqrt{n}$ error bars.

Table 4
Cumulated Flux Distribution of Interstellar Grains Derived in This Paper

Mass (kg) (1)	Flux ($\geqslant m$) (m^{-2} s^{-1}) (2)	Err Y+ (m^{-2} s^{-1}) (3)	Err Y− (m^{-2} s^{-1}) (4)
2.05E-19	7.03E-05	7.26E-05	6.81E-05
6.47E-19	7.03E-05	7.26E-05	6.81E-05
2.05E-18	6.97E-05	7.19E-05	6.75E-05
6.47E-18	6.06E-05	6.27E-05	5.86E-05
2.05E-17	4.75E-05	4.93E-05	4.56E-05
6.47E-17	3.69E-05	3.85E-05	3.53E-05
2.05E-16	2.59E-05	2.73E-05	2.46E-05
6.47E-16	1.63E-05	1.74E-05	1.52E-05
2.05E-15	4.42E-06	4.98E-06	3.86E-06
6.47E-15	1.50E-06	1.82E-06	1.17E-06
2.05E-14	4.99E-07	6.87E-07	3.10E-07
6.47E-14	3.56E-07	5.16E-07	1.97E-07
2.05E-13	7.13E-08	1.43E-07	0.00E+00

Note. The data are shown in Figure 7. Column (1) lists the grain mass, Column (2) lists the cumulated flux of grains larger than the given mass, and Columns (3) and (4) list the $\sqrt{n}$ errors.

APPENDIX

Figure 8 shows the *Ulysses* interstellar dust data set used in this paper for three different grain size intervals with approximately equal numbers of particles in each figure.

The data shown in Figures 6 and 7 are listed in Tables 3–4.

REFERENCES

Altobelli, N., Dikarev, V., Kempf, S., et al. 2007, JGR, 112, A07105
Altobelli, N., Grün, E., & Landgraf, M. 2006, A&A, 448, 243
Altobelli, N., Kempf, S., Krüger, H., et al. 2005, JGR, 110, A07102
Altobelli, N., Kempf, S., Landgraf, M., et al. 2003, JGR, 108, 7
Altobelli, N., Moissl, R., Krüger, H., Landgraf, M., & Grün, E. 2004, P&SS, 52, 1287
Altobelli, N., Postberg, F., Kimura, H., et al. 2015, Sci, submitted
Auer, S. 2001, in Interplanetary Dust, ed. E. Grün et al. (Berlin: Springer), 385
Baggaley, W. J., Marsh, S. H., & Close, S. 2007, in Dust in Planetary Systems ESA SP-643, Interstellar Meteors, ed. H. Krüger & A. L. Graps (Tvoordijk, Netherlands: ESA), 27
Baggaley, W. J., & Neslušan, L. 2002, A&A, 382, 1118
Baguhl, M., Grün, E., Hamilton, D. P., et al. 1995a, SSRv, 72, 471
Baguhl, M., Grün, E., & Landgraf, M. 1996, SSRv, 78, 165
Baguhl, M., Grün, E., Linkert, G., Linkert, D., & Siddique, N. 1993, P&SS, 41, 1085
Baguhl, M., Hamilton, D. P., Grün, E., et al. 1995b, Sci, 268, 1016
Belheouane, S., Zaslavsky, A., Meyer-Vernet, N., et al. 2012, SoPh, 281, 501
Bertaux, J. L., & Blamont, J. F. 1976, Natur, 262, 263
Czechowski, A., & Mann, I. 2003a, A&A, 410, 165
Czechowski, A., & Mann, I. 2003b, JGR, 108, 8038
Dietzel, H., Eichhorn, G., Fechtig, H., et al. 1973, JPhE, 6, 209
Draine, B. T. 2003, ARA&A, 41, 241
Draine, B. T. 2009, SSRv, 143, 333
Draine, B. T. 2011, Physics of the Interstellar and Intergalactic Medium (Princeton, NJ: Princeton Univ. Press)
Drolshagen, G., Svedhem, H., Grün, E., Grafodatsky, O., & Prokopiev, U. 1999, AdSpR, 23, 123
Fechtig, H., Grün, E., & Kissel, J. 1978, in Cosmic Dust, ed. J. A. M. McDonnell (New York: Wiley), 607
Flandes, A., Krüger, H., Hamilton, D. P., et al. 2011, P&SS, 59, 1455
Friichtenicht, J. F., & Slattery, J. C. 1963, Ionization Associated with Hypervelocity Impact, Tech. Rep., NASA Technical Note D-2091
Frisch, P. C., Bzowski, M., Livadiotis, G., et al. 2013, Sci, 341, 1080
Frisch, P. C., Dorschner, J., Geiß, J., et al. 1999, ApJ, 525, 492
Frisch, P. C., Redfield, S., & Slavin, J. D. 2011, ARA&A, 49, 237
Frisch, P. C., & Slavin, J. D. 2003, ApJ, 594, 844
Frisch, P. C., & Slavin, J. D. 2013, EP&S, 65, 175
Göller, J. R., & Grün, E. 1985, in Properties and Interaction of Interplanetary Dust, ed. R. H. Giese & P. Lamy (Dordrecht: Reidel), 113
Göller, J. R., & Grün, E. 1989, P&SS, 37, 1197
Graps, A. L., Grün, E., Svedhem, H., et al. 2000, Natur, 405, 48
Grün, E., Baguhl, M., Divine, N., et al. 1995a, P&SS, 43, 971
Grün, E., Baguhl, M., Hamilton, D. P., et al. 1995b, P&SS, 43, 941
Grün, E., Dikarev, V., Frisch, P. C., et al. 2004, in Astrophysics of Dust 309 ASP Conf. Ser., Dust in Interplanetary Space and in the Local Galactic Environment, ed. A. N. Witt, G. C. Clayton & B. T. Draine (San Francisco, CA: ASP), 245
Grün, E., Fechtig, H., Hanner, M. S., et al. 1992a, SSRv, 60, 317
Grün, E., Fechtig, H., Kissel, J., et al. 1992b, A&AS, 92, 411
Grün, E., Gustafson, B. E., Mann, I., et al. 1994, A&A, 286, 915
Grün, E., Krüger, H., Graps, A., et al. 1998, JGR, 103, 20011
Grün, E., & Landgraf, M. 2000, JGR, 105, 10291
Grün, E., Staubach, P., Baguhl, M., et al. 1997, Icar, 129, 270
Grün, E., Zook, H. A., Baguhl, M., et al. 1993, Natur, 362, 428
Gustafson, B. A. S. 1994, AREPS, 22, 553
Hamilton, D. P., Grün, E., & Baguhl, M. 1996, in Physics, Chemistry and Dynamics of Interplanetary Dust ASP Conf. Ser. 104, Electromagnetic Escape of Dust from the Solar System, ed. B. A. S. Gustafson & M. S. Hanner (San Francisco, CA: ASP), 31
Heerikhuisen, J., & Pogorelov, N. V. 2011, ApJ, 738, 29
Hillier, J. K., Sestak, S., Green, S. F., et al. 2009, P&SS, 57, 2081
Hillier, J. K., Sternovsky, Z., Armes, S. P., et al. 2014, P&SS, 97, 9
Kempf, S., Beckmann, U., Srama, R., et al. 2006, P&SS, 54, 999
Kempf, S., Srama, R., Altobelli, N., et al. 2004, Icar, 171, 317

Kimura, H., & Mann, I. 1999, in Meteroids 1998, ed. W. J. Baggaley & V. Porubcan (Bratislava, Slovakia: Astronomical Institute of the Slovak Academy of Sciences), 283
Kimura, H., Mann, I., & Jessberger, E. K. 2003a, ApJ, 582, 846
Kimura, H., Mann, I., & Jessberger, E. K. 2003b, ApJ, 583, 314
Krüger, H., Altobelli, N., Anweiler, B., et al. 2006a, P&SS, 54, 932
Krüger, H., Dikarev, V., Anweiler, B., et al. 2010, P&SS, 58, 951
Krüger, H., Graps, A. L., Hamilton, D. P., et al. 2006b, P&SS, 54, 919
Krüger, H., & Grün, E. 2009, SSR, 143, 347
Krüger, H., Grün, E., Landgraf, M., et al. 1999a, P&SS, 47, 363
Krüger, H., Grün, E., Landgraf, M., et al. 2001, P&SS, 49, 1303
Krüger, H., Grün, E., Linkert, D., Linkert, G., & Moissl, R. 2005, P&SS, 53, 1109
Krüger, H., Krivov, A. V., & Grün, E. 2000, P&SS, 48, 1457
Krüger, H., Krivov, A. V., Hamilton, D. P., & Grün, E. 1999b, Natur, 399, 558
Krüger, H., Krivov, A. V., SremčeviĆ, M., & Grün, E. 2003, Icar, 164, 170
Krüger, H., Landgraf, M., Altobelli, N., & Grün, E. 2007, SSRv, 130, 401
Lallement, R., & Bertaux, J. L. 2014, A&A, 565, A41
Lallement, R., & Bertin, P. 1992, A&A, 266, 479
Landgraf, M. 1998, PhD thesis, Ruprecht-Karls-Univ.
Landgraf, M. 2000, JGR, 105, 10303
Landgraf, M., Augustsson, K., Grün, E., & Gustafson, B. A. S. 1999, Sci, 286, 2319
Landgraf, M., Baggeley, W. J., Grün, E., Krüger, H., & Linkert, G. 2000, JGR, 105, 10343
Landgraf, M., Krüger, H., Altobelli, N., & Grün, E. 2003, JGR, 108, 8030
Linde, T. J., & Gombosi, T. I. 2000, JGR, 105, 10411
Mann, I. 2010, ARA&A, 48, 173
Mann, I., & Kimura, H. 2000, JGR, 105, 10317
Mathis, J. S. 2000, JGR, 105, 10269
Mathis, J. S., Rumpl, W., & Nordsieck, K. H. 1977, ApJ, 217, 425
McComas, D. J., Alexashov, D., Bzowski, M., et al. 2012, Sci, 336, 1291
McComas, D. J., Bzowski, M., Frisch, P., et al. 2015, ApJ, 801, 28
Misconi, N. Y. 1993, JGR, 98, 18951
Möbius, E., Bzowski, M., Chalov, S., et al. 2004, A&A, 426, 897
Raizer, Y. P. 1960, Sov. Phys. JETP, 10, 411
Redfield, S., & Linsky, J. L. 2008, ApJ, 673, 283
Slavin, J. D., & Frisch, P. C. 2008, A&A, 491, 53
Slavin, J. D., Frisch, P. C., Heerikhuisen, J., et al. 2010, in AIP Conf. Proc. 1216, Twelfth Int. Solar Wind Conf. 1216, Exclusion of Tiny Interstellar Dust Grains From the Heliosphere, ed. M. Maksimovic, K. Issatauer, N. Meyer-Vernet, M. Moncuquet & F. Pantellini (New York: AIP), 497
Slavin, J. D., Frisch, P. C., Müller, H.-R., et al. 2012, ApJ, 760, 46
Srama, R., Ahrens, T. J., Altobelli, N., et al. 2004, SSRv, 114, 465
Sterken, V. J. 2012, PhD thesis, IGEP, Univ. Braunschweig, MPIK, IRS, Univ. Stuttgart
Sterken, V. J., Altobelli, N., Kempf, S., et al. 2012, A&A, 538, A102
Sterken, V. J., Altobelli, N., Kempf, S., et al. 2013a, A&A, 552, A130
Sterken, V. J., Moragas-Klostermeyer, G., Hillier, J. K., et al. 2013b, in Dusty Visions Workshop, Calibration of Impact Ionization Dust Detectors with Porous or Fluffy Dust Particles(Univ. Stuttgart), 1
Sterken, V. J., Strub, P., Krüger, H., von Steiger, R., & Frisch, P. 2015, ApJ, 812, 141
Strub, P., Krüger, H., & Sterken, V. J. 2015, ApJ, 812, 140
Strub, P., Sterken, V. J., Krüger, H., Grün, E., & Horányi, M. 2011, in AIP Conf. Ser. 1397, Interstellar Dust Flow through the Solar System, ed. V. Y. Nosenko et al. (Melville, NY: AIP), 385
Stübig, M. 2002, PhD thesis, Ruprecht-Karls-Univ.
Stübig, M., Schäfer, G., Ho, T.-M., Srama, R., & Grün, E. 2001, P&SS, 49, 853
Svestka, J., Auer, S., Baguhl, M., & Grün, E. 1996, in Physics, Chemistry and Dynamics of Interplanetary Dust ASP Conf. Ser. 104, Measurements of Dust Electric Charges by the Ulysses and Galileo Dust Detectors, ed. B. A. Gustafson & M. S. Hanner (San Francisco, CA: ASP), 481
Taylor, A. D., Baggeley, W. J., & Steel, D. I. 1996, Natur, 380, 323
Wang, S., Li, A., & Jiang, B. W. 2014, P&SS, 100, 32
Wehry, A., Krüger, H., & Grün, E. 2004, A&A, 419, 1169
Wehry, A., & Mann, I. 1999, A&A, 341, 296
Wenzel, K., Marsden, R., Page, D., & Smith, E. 1992, A&AS, 92, 207
Westphal, A. J., Stroud, R. M., Bechtel, H. A., et al. 2014, Sci, 345, 786
Willis, M. J., Burchell, M., Ahrens, T. J., Krüger, H., & Grün, E. 2005, Icar, 176, 440
Witte, M. 2004, A&A, 426, 835
Witte, M., Banaszkiewicz, H., & Rosenbauer, H. 1996, SSRv, 78, 289
Wolf, H., Rhee, J., & Berg, O. E. 1976, in Interplanetary Dust and Zodiacal Light, Vol. 48, ed. H. Elsässer & H. Fechtig (Berlin: Springer), 165
Wood, B. E., Müller, H.-R., & Witte, M. 2015, ApJ, 801, 62
Zook, H. A., Grün, E., Baguhl, M., et al. 1996, Sci, 274, 1501